Amygdala-hippocampal innervation modulates stress-induced depressive-like behaviors through AMPA receptors

Hui Ma[a,b], Chenyang Li[a], Jinpeng Wang[a], Xiaochen Zhang[a], Mingyue Li[c], Rong Zhang[a], Zhuo Huang[b], and Yong Zhang[a,1]

[a]Neuroscience Research Institute and Department of Neurobiology, School of Basic Medical Sciences, Peking University Health Science Center, Key Laboratory for Neuroscience, Ministry of Education/National Health Commission of People's Republic of China, IDG/McGovern Institute for Brain Research at Peking University, 100083 Beijing, People's Republic of China; [b]Department of Pathology and Laboratory Medicine, Perelman School of Medicine, University of Pennsylvania, Philadelphia, PA 19104; and [c]State Key Laboratory of Natural and Biomimetic Drugs, Key Laboratory of Carcinogenesis and Translational Research (Ministry of Education), Beijing Key Laboratory of Protein Posttranslational Modifications and Cell Function, Department of Molecular and Cellular Pharmacology, School of Pharmaceutical Sciences, Peking University Health Science Center, 100083 Beijing, People's Republic of China

Edited by Jeremy Nathans, Johns Hopkins University School of Medicine, Baltimore, MD, and approved January 4, 2021 (received for review October 27, 2020)

Chronic stress is one of the most critical factors in the onset of depressive disorders; hence, environmental factors such as psychosocial stress are commonly used to induce depressive-like traits in animal models of depression. Ventral CA1 (vCA1) in hippocampus and basal lateral amygdala (BLA) are critical sites during chronic stress-induced alterations in depressive subjects; however, the underlying neural mechanisms remain unclear. Here we employed chronic unpredictable mild stress (CUMS) to model depression in mice and found that the activity of the posterior BLA to vCA1 (pBLA-vCA1) innervation was markedly reduced. Mice subjected to CUMS showed reduction in dendritic complexity, spine density, and synaptosomal AMPA receptors (AMPARs). Stimulation of pBLA-vCA1 innervation via chemogenetics or administration of cannabidiol (CBD) could reverse CUMS-induced synaptosomal AMPAR decrease and efficiently alleviate depressive-like behaviors in mice. These findings demonstrate a critical role for AMPARs and CBD modulation of pBLA-vCA1 innervation in CUMS-induced depressive-like behaviors.

depression | AMPAR | chronic stress | pBLA-vCA1 | CBD

Major depression or major depressive disorder (MDD) is one of the most common and disabling mental disorders worldwide and is characterized by episodes of depressed mood, decreased drive, and loss of interest and pleasure (1, 2). Although MDD is multifactorial and heterogeneous by nature, negative stimuli such as stress are strongly implicated in MDD (3–5). The CA1 area in hippocampus has been one of the most intensively studied brain regions in depression research. Patients with MDD show a marked reduction in left CA1 volume (6). Rodents subjected to stress also have impaired spike timing-dependent long-term depression (LTD), as well as decreased spine density and down-regulated synaptic transmission in ventral CA1 (vCA1) pyramidal neurons (7, 8).

vCA1 shares robust reciprocal projections with the basal lateral amygdala (BLA), a pivotal site underlying stress-induced emotional disorders. Based on morphological and genotypic distinction, the BLA has been divided into two subregions, anterior BLA (aBLA) and posterior BLA (pBLA) (9), both of which can be activated by negative (10–12) and positive (13, 14) emotion-associated events. Under physiological conditions, pBLA has a stronger monosynaptic connection to vCA1 than aBLA (15). Furthermore, optogenetic activation of the pBLA-vCA1 circuit can reduce anxiety-like behaviors (16). However, the mechanisms through which the pBLA-vCA1 circuit impacts the pathogenesis of depression remain unclear.

AMPA receptors (AMPARs) play a critical role in synaptic plasticity, and dysfunction in AMPARs or proteins that regulate AMPAR trafficking has been linked to various neurological and psychiatric disorders (17). Stress selectively decreases expression of GluA1, an AMPAR subunit, in vCA1 and impairs AMPAR-mediated synaptic excitation (8). Antidepressants fluoxetine and reboxetine can increase the expression of GluA1/GluA3 in hippocampus and GluA2/GluA4 in prefrontal cortex (PFC), respectively (18). The cannabinoid system also plays an important role in regulation of mood and depression. Synthetic cannabinoids that activate cannabinoid type-1 (CB_1) and cannabinoid type-2 (CB_2) receptors can alleviate depressive-like symptoms in animal models (19, 20). Recently, cannabidiol (CBD), a nonpsychotomimetic component of *Cannabis sativa*, has emerged as a promising compound, since it exerts large-spectrum therapeutic potential in human mental disorders such as psychosis, anxiety, and depression (21). It has been reported that chronic CBD treatment induces behavioral and synaptic changes in stressed mice through CB_1/CB_2 receptor activation (22), but its acute antidepressant properties and underlying mechanisms have not been completely investigated.

In the present study, we employed a chronic unpredictable mild stress (CUMS) procedure to induce a model of depression in mice and found that CUMS exposure resulted in decreased activity in pBLA-vCA1 innervation, while chemogenetic activation of pBLA-vCA1 input could reverse CUMS-induced behavior deficits. CUMS led to reduction in dendritic complexity, spine density, and synaptosomal AMPARs. Moreover, inhibition of AMPAR activity via application of DNQX under subthreshold

Significance

Basal lateral amygdala and ventral CA1 are critical sites during chronic stress-induced depression. Here we demonstrated that AMPARs mediated weakening of pBLA-vCA1 innervation in mice subjected to CUMS. Stimulation of pBLA-vCA1 innervation via chemogenetics or administration of cannabidiol (CBD) could reverse synaptosomal AMPAR decrease and alleviate CUMS-induced depressive-like behaviors. These findings highlighted the importance of AMPARs and the pBLA-vCA1 innervation in an animal model of depression and revealed the potential for CBD in major depression treatment.

Author contributions: H.M., R.Z., Z.H., and Y.Z. designed research; H.M., C.L., J.W., and X.Z. performed research; and H.M., M.L., and Y.Z. wrote the paper.

The authors declare no competing interest.

This article is a PNAS Direct Submission.

[1]To whom correspondence may be addressed. Email: yongzhang@hsc.pku.edu.cn.

This article contains supporting information online at https://www.pnas.org/lookup/suppl/doi:10.1073/pnas.2019409118/-/DCSupplemental.

Published February 1, 2021.

stress conditions could induce depressive-like behaviors. Acute CBD administration reversed CUMS-induced reduction in mature spine density and synaptosomal AMPAR level in vCA1, and, more importantly, alleviated depressive-like behaviors. In summary, our study sheds light on the mechanisms underlying depressive-like behavior and advances our understanding of the complex pathology of depression.

Results

Activity of vCA1 Excitatory Neurons Plays a Critical Role in CUMS-Induced Depressive-Like Behaviors. CUMS is a widely used animal model of depression that recapitulates many features of the disease (23); hence, we employed a CUMS procedure to induce a model of depression in mice. After 4 wk CUMS experience, mice displayed typical depressive-like phenotypes as evidenced by sucrose preference test (SPT), novelty-suppressed feeding test (NSFT), and forced swim test (FST; Fig. 1*A* and *SI Appendix*, Fig. S1 *A–C*). Since the ventral hippocampus (vHPC) has been strongly implicated in maladapted emotional states such as depression (24), we first examined the neuronal activity via c-Fos expression in vHPC in mice subjected to CUMS (Fig. 1*B* and *SI Appendix*, Fig. S1 *D* and *E*). Fewer c-Fos–positive neurons (marked by NeuN) were detected in vCA1 of CUMS mice after FST compared with the no-stress (NS) group ($F_{2,\ 24} = 23.44$, $P < 0.0001$; Fig. 1 *C*, *Top*), and there was a negative correlation between the c-Fos level in vCA1 and the immobility time in the FST ($r = -0.8982$, $P = 0.0004$; Fig. 1 *C*, *Bottom*). To further explore the identity of the neurons activated after FST, the excitatory neuronal marker CaMKIIα and the inhibitory neuronal markers GAD67 or parvalbumin (PV) were costained with c-Fos. As shown in Fig. 1*D*, robust coexpression between c-Fos and CaMKIIα was detected, along with only a small fraction showing coexpression between c-Fos and GAD67 and almost no coexpression between c-Fos and PV. These results indicated CUMS exposure significantly reduced the activity of the excitatory neurons in vCA1 during FST. To further demonstrate the critical role of vCA1 in CUMS-induced depressive-like behaviors, we bilaterally expressed hM3Dq, a designer receptor exclusively activated by designer drugs, via CaMKIIα promoter-driven adeno-associated virus (AAV) infection in vCA1 1 wk before mice were subjected to CUMS. The control groups received the same viral vector carrying only the morphology marker AAV-CaMKIIα-mCherry. Immunostaining results showed hM3Dq expression was confined to vCA1 (Fig. 1*E*). Application of clozapine N-oxide (CNO), an hM3Dq agonist, via intraperitoneal (i.p.) injection led to a significant increase in vCA1 neuronal activity compared with control, which was evidenced by increased total number ($t_{13} = 3.885$, $P = 0.0019$; Fig. 1 *F*, *Bottom Left*) and proportion ($t_{13} = 6.278$, $P < 0.0001$; Fig. 1 *F*, *Bottom Right*) of c-Fos–positive neurons. Activation of vCA1 excitatory neurons with CNO injection in mice subjected to CUMS resulted in increased sucrose preference in the SPT ($F_{2,42} = 5.208$, $P = 0.0095$; Fig. 1*G*), reduced latency to feeding in the NSFT ($F_{2,42} = 3.288$, $P = 0.0472$; Fig. 1*H*), reduced immobility time (hM3Dq effect, $F_{2,42} = 5.916$, $P = 0.0054$; CNO effect, $F_{1,42} = 8.384$, $P = 0.006$; Fig. 1 *I*, *Left*), and increased latency to immobility in the FST (hM3Dq effect, $F_{2,42} = 8.046$, $P = 0.0011$; CNO effect, $F_{1,42} = 4.946$, $P = 0.0316$; Fig. 1 *I*, *Right*). These results indicate that CUMS-induced depressive-like behaviors arise due to decreased activity of excitatory neurons in vCA1.

CUMS Induces Depressive-Like Behavior through pBLA-vCA1 Innervation. To investigate the neural circuits in CUMS-induced depressive-like behaviors, we set up to explore the upstream nucleus that projects to vCA1. Fluorescent gold (FG), a retrograde tracer, was injected into vCA1 to identify the regions projecting to vCA1 (*SI Appendix*, Fig. S2*A*). Notably, FG-positive neurons were most prominent in pBLA but not in aBLA ($t_4 = 7.442$, $P = 0.0017$; *SI Appendix*, Fig. S2*B*), and the number of FG, c-Fos, and NeuN triple-positive cells in the CUMS group was significantly lower than that in the NS group ($t_8 = 3.34$, $P = 0.0003$; *SI Appendix*, Fig. S2 *C* and *D*, *Top*). Interestingly, the majority of c-Fos–positive neurons in pBLA projected to vCA1 in both NS and CUMS groups (FG effect, $F_{1,16} = 519.6$, $P < 0.0001$; *SI Appendix*, Fig. S2 *D*, *Bottom*). Furthermore, FG and c-Fos double-positive neurons coexpressed CaMKIIα, but not GAD67 or PV ($F_{2,6} = 219.1$, $P < 0.0001$; *SI Appendix*, Fig. S2*E*), indicating that they were likely excitatory neurons. To further confirm the innervation from pBLA to vCA1, we took the reciprocal approach to trace the downstream targets of pBLA. An inducible transsynaptic anterograde tracer, AAV2/1-Ef1a-DIO-mCherry-WPRE, was injected into the pBLA of CaMKIIα-Cre mice 1 wk before the CUMS procedure. Robust mCherry expression was observed in vCA1, while little expression was detected in aBLA and almost no expression in dCA1 (Fig. 2*A*), which indicates that vCA1 is a major projection target of pBLA. The number of mCherry, c-Fos, and NeuN triple-positive cells in the CUMS group was significantly lower than that in the NS group ($t_8 = 9.037$, $P < 0.0001$; Fig. 2 *B* and *C*, *Top*), which suggests that CUMS leads to a decreased activity in vCA1 neurons receiving inputs from pBLA ($F_{1,16} = 135.7$, $P < 0.0001$; Fig. 2 *C*, *Bottom*). These results show decreased activity of the pBLA-vCA1 innervation correlates with CUMS-induced depressive-like behaviors, which is consistent with previous findings that BLA-vHPC connections are heavily involved in anxiety-related behaviors (25).

To further explore the roles that pBLA-vCA1 innervation plays in an animal model of depression, we investigated whether activating this excitatory circuit could promote resilience to CUMS exposure. The intersectional Cre-ON chemogenetic strategy was employed by injecting Cre-dependent AAV2/9-hSyn-DIO-hM3D(Gq)-GFP into pBLA and a retrograde CaMKIIα promoter-driven AAV2/Retro-CaMKIIα-mCherry-Cre in vCA1 1 wk before the CUMS procedure; AAV2/9-hSyn-DIO-GFP was injected into pBLA to serve as the control (Fig. 2 *D* and *E*). CNO injection in CaMKIIα-Cre mice led to increased activity of pBLA ($t_{13} = 4.371$, $P = 0.0008$) and vCA1 ($t_{13} = 3.936$, $P = 0.0017$) excitatory neurons (Fig. 2 *F* and *G*). More importantly, chemogenetic activation of the pBLA-vCA1 innervation dramatically reversed the behavioral deficits in mice subjected to CUMS (sucrose preference, hM3Dq effect, $F_{2,42} = 17.09$, $P < 0.0001$; CNO effect, $F_{1,42} = 5.845$, $P = 0.02$; latency to feeding, hM3Dq effect, $F_{2,42} = 4.978$, $P = 0.0115$; immobility time, $F_{2,42} = 4.371$, $P = 0.0189$; latency to immobility, hM3Dq effect, $F_{2,42} = 7.868$, $P = 0.0013$; Fig. 2 *H–J*), which indicates that activation of pBLA-vCA1 innervation exerts an antidepressant effect.

Mice that underwent 2 to 4 wk of CUMS treatment showed a significantly reduced sucrose preference; however, 1 wk of CUMS treatment was insufficient to produce changes in sucrose preference (*SI Appendix*, Fig. S3*A*). To further confirm the roles of pBLA-vCA1 innervation in the mouse model of depression, we examined whether inhibiting pBLA-vCA1 innervation could induce depressive-like behaviors in mice subjected to subthreshold unpredictable mild stress (SUMS). Virus carrying Cre-dependent inhibitory designer receptor, AAV2/9-hSyn-DIO-hM4D(Gi)-GFP, was locally injected into pBLA, and retrograde Cre-recombinase was injected into vCA1, 1 wk before the subthreshold stress procedure (*SI Appendix*, Fig. S3 *B* and *C*). We found chemogenetic inhibition of the pBLA-vCA1 innervation led to decreased sucrose preference (hM4Di effect, $F_{1,28} = 5.143$, $P = 0.0313$; CNO effect, $F_{1,\ 28} = 4.777$, $P = 0.0374$), increased latency to feeding (CNO effect, $F_{1,28} = 6.197$, $P = 0.0190$), increased immobility time (hM4Di effect, $F_{1,\ 28} = 4.493$, $P = 0.0430$), and reduced latency to immobility (hM4Di effect, $F_{1,28} = 4.395$, $P = 0.0452$), which recapitulates the CUMS phenotypes (*SI Appendix*, Fig. S3 *D–F*). These results demonstrate that inhibition of pBLA-vCA1 innervation could exacerbate depressive-like responses

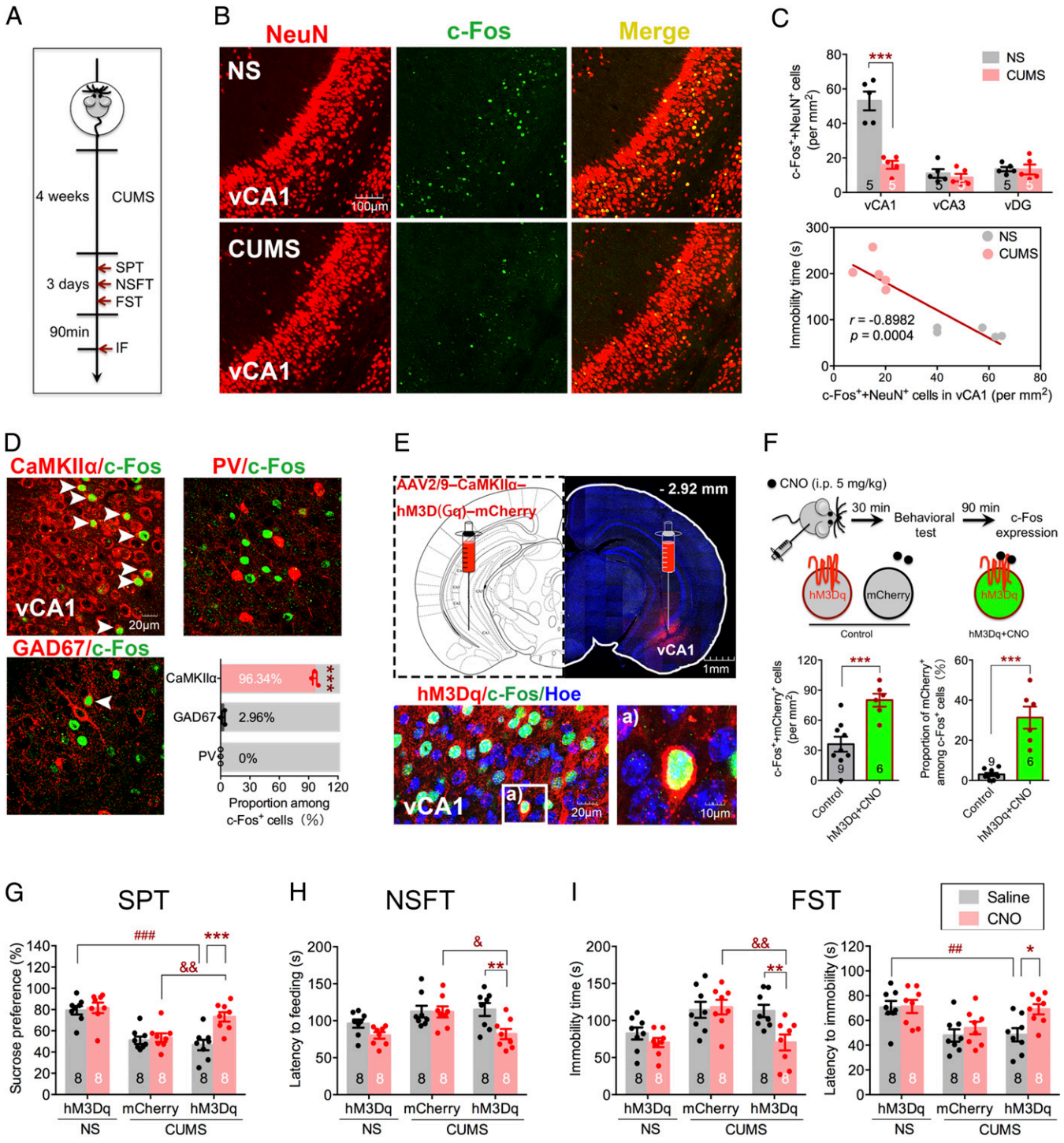

Fig. 1. CUMS leads to decreased neuronal activity in vCA1. (*A*) Experimental design. IF, immunofluorescence staining. (*B*) Representative immunostaining images of NeuN (red) and c-Fos (green) in vCA1 of NS and CUMS groups, respectively. (*C*, *Top*) Quantification of c-Fos and NeuN double-positive cells in vCA1, vCA3, and vDG (two-way ANOVA with Sidak's post hoc test, $^{***}P < 0.001$). (*C*, *Bottom*) Relationship between double-positive cells in vCA1 and immobility time in FST (Pearson's correlation, $r = -0.8982$, $P = 0.0004$; $n = 5$ per group). (*D*) Representative images and quantification of CaMKIIα-, GAD67-, or PV-positive cells colabeled with c-Fos–positive cells in vCA1 of NS group. White arrowheads indicate colabeled cells (one-way ANOVA with Tukey's post hoc test, $^{***}P < 0.001$; $n = 3$ per group). (*E*, *Top*) Representative images of hM3Dq injection sites in vCA1 (red). (*E*, *Bottom*) Representative images of hM3Dq (red), c-Fos (green), and Hoechst (blue) colabeled in vCA1. (*F*, *Top*) Diagram of CNO (5 mg/kg) injection to increase neural activity. (*Bottom Left*) Quantification of c-Fos and mCherry double-positive cells in vCA1. (*Bottom Right*) Proportion of double-positive cells among c-Fos–positive cells (unpaired Student's *t* test, $^{***}P < 0.001$). (*G*) Sucrose preference in SPT. (*H*) Latency to feeding in NSFT. (*I*, *Left*) Immobility time in FST. (*I*, *Right*) Latency to immobility in FST (two-way ANOVA with Sidak's post hoc test, $^{*}P < 0.05$, $^{**}P < 0.01$, $^{***}P < 0.001$, $^{\#\#}P < 0.01$, $^{\#\#\#}P < 0.001$, $^{\&}P < 0.05$, $^{\&\&}P < 0.01$). Data are presented as the mean ± SEM.

to stress. Altogether, our data suggest that pBLA-vCA1 innervation plays an essential role in CUMS-induced depressive-like behaviors.

AMPARs Mediate CUMS-Induced Weakening of pBLA-vCA1 Innervation. To further examine the structural and functional changes in the pBLA-vCA1 innervation in this mouse model of depression, we

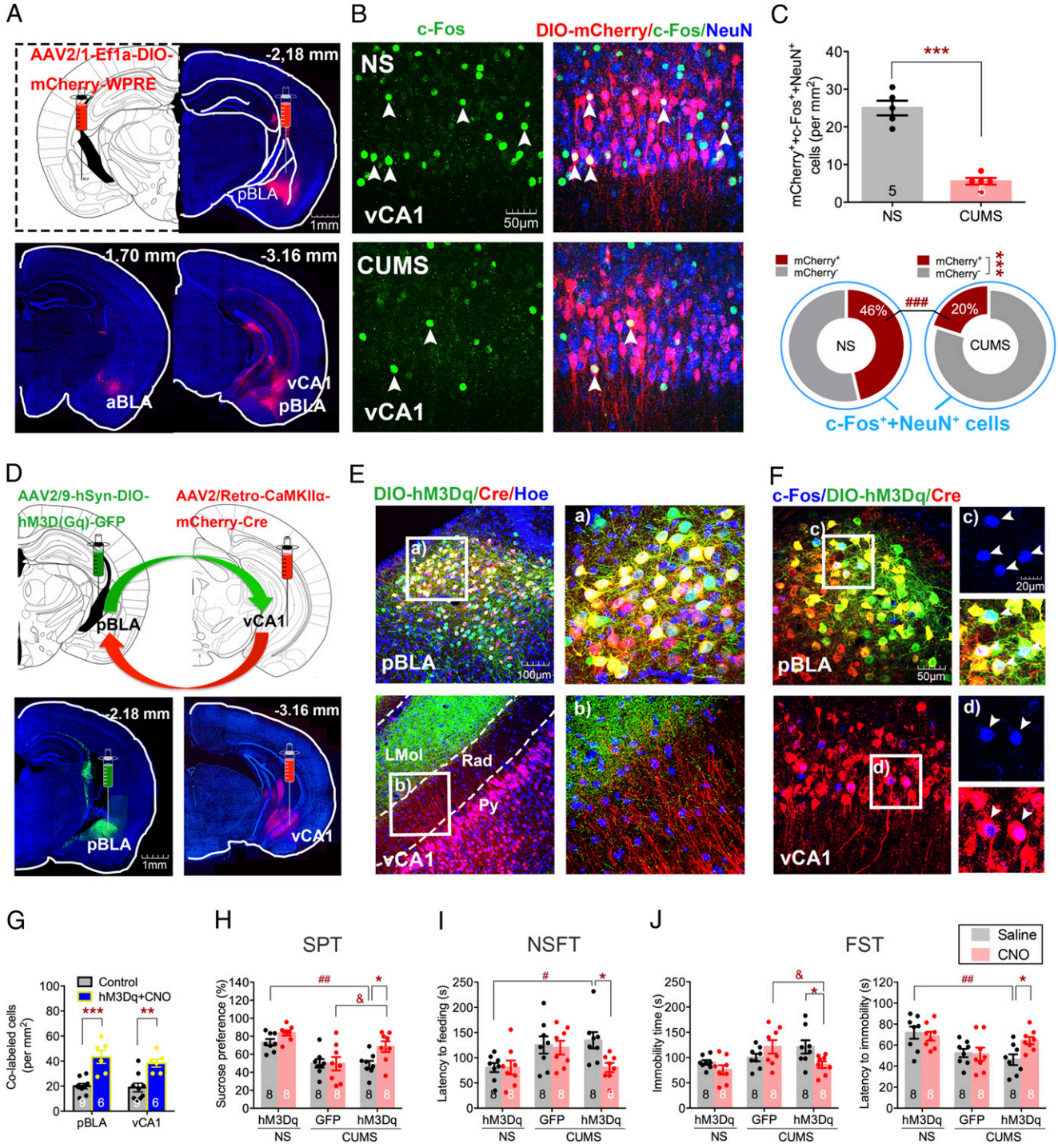

Fig. 2. pBLA-vCA1 innervation shows a decreased activity in mice subjected to CUMS, and chemogenetic activation of pBLA-vCA1 innervation exerts antidepressant effects. (*A*) Representative images of Cre-dependent mCherry injection sites in pBLA (red) and mCherry-expressed in aBLA and vCA1 of CaMKIIα-Cre mice. (*B*) Representative images of DIO-mCherry (red), c-Fos (green), and NeuN (blue) colabeled in vCA1 of NS and CUMS groups, respectively. (*C*, *Top*) Quantification of DIO-mCherry, c-Fos, and NeuN triple-positive cells in vCA1 (unpaired Student's *t* test, $^{***}P < 0.001$). (*C*, *Bottom*) Proportion of mCherry-positive or mCherry-negative cells colabeled with c-Fos–positive neurons (two-way ANOVA with Sidak's post hoc test, $^{***}P < 0.001$, $mCherry^+$+c-Fos^++$NeuN^+$ vs. $mCherry^-$+c-Fos^++$NeuN^+$ in CUMS group; $^{\#\#\#}P < 0.001$, $mCherry^+$+c-Fos^++$NeuN^+$ of CUMS vs. $mCherry^+$+c-Fos^++$NeuN^+$ of NS group; $n = 5$ per group). (*D*) Representative images of DIO-hM3Dq and CaMKIIα-Cre injection sites and expression in pBLA (green; *Left*) and vCA1 (red; *Right*), respectively. (*E*) Representative images of DIO-hM3Dq (green), CaMKIIα-Cre (red) expression, and Hoechst (blue) in pBLA and vCA1, respectively. Rad, stratum radiatum of the hippocampus; Py, pyramidal cell layer of the hippocampus; LMol, lacunosum moleculare layer of the hippocampus. (*F*, *Top*) Representative images of c-Fos (blue), DIO-hM3Dq (green), and CaMKIIα-Cre (red) colabeled cells in the pBLA from mice treated with CNO. (*F*, *Bottom*) Representative images of c-Fos (blue) and CaMKIIα-Cre (red) colabeled cells in the vCA1 of hM3Dq-expressing mice treated with CNO. White arrowheads indicate c-Fos positive (*Top*) and colabeled (*Bottom*) cells. (*G*) Quantification of colabeled cells in pBLA and vCA1 (unpaired Student's *t* test, $^{**}P < 0.01$, $^{***}P < 0.001$). (*H*) Sucrose preference in SPT. (*I*) Latency to feeding in NSFT. (*J*, *Left*) Immobility time in FST. (*J*, *Right*) Latency to immobility in FST (two-way ANOVA with Sidak's post hoc test, $^{*}P < 0.05$, $^{\#}P < 0.05$, $^{\#\#}P < 0.01$, $^{\&}P < 0.05$). Data are presented as the mean ± SEM.

carried out projection-specific neuronal morphology reconstruction using Cre/loxP-based Supernova vectors (26) to measure dendrite complexity and spine density. AAV2/1-hSyn-Cre, a transsynaptic anterograde Cre recombinase, was injected into pBLA, and Supernova vectors AAV2/9-TRE-DIO-FLPo and AAV2/9-TRE-fDIO-GFP-IRES-Tta were injected into vCA1 1 wk before the CUMS procedure (Fig. 3*A*). We observed a dramatic decrease in dendritic complexity (main effect of CUMS, $F_{1,196} = 10.12$, $P = 0.0017$; Fig. 3 *B* and *C*) and in dendritic spine density ($t_{88} = 2.746$, $P = 0.0073$; $t_{88} = 3.043$, $P = 0.0031$; Fig. 3*D*) in the CUMS group compared with control. We next investigated molecular changes in vCA1 by detecting AMPARs, PSD95, and CaMKIIα via Western blot. There was a significant decrease in the levels of synaptosomal GluA1 ($t_{10} = 2.767$, $P = 0.0199$) and PSD95 ($t_{10} = 4.175$, $P = 0.0019$), but not GluA2 ($t_{10} = 1.401$, $P = 0.1913$), in the CUMS group (Fig. 3 *E* and *F*). It has been well documented that phosphorylation of GluA1 plays critical roles in AMPAR function and trafficking, so we next examined the phosphorylation level of GluA1. Phosphorylation at both S831 ($t_{10} = 2.516$, $P = 0.0306$) and S845 ($t_{10} = 2.595$, $P = 0.0267$) of GluA1 was significantly decreased in vCA1 in mice subjected to CUMS (Fig. 3*F*). There was also a strong negative correlation between the level of synaptosomal GluA1 and immobility time in the FST ($r = -0.6307$, $P = 0.0279$; Fig. 3*G*). In addition, inhibition of pBLA-vCA1 in mice subjected to subthreshold stress led to synaptosomal GluA1 level reduction ($F_{1,12} = 23.99$, $P = 0.0004$; Fig. 3 *H–K*). On the contrary, chemogenetic activation of pBLA-vCA1 innervation could restore synaptosomal GluA1 level ($F_{2,18} = 44.28$, $P < 0.0001$) and phosphorylation at S831 in GluA1 ($F_{2,18} = 10.80$, $P = 0.0008$; Fig. 3 *L–O*) and reverse behavior deficits in mice subjected to CUMS (Fig. 2 *H–J*). These data suggest that the behavioral deficits induced by CUMS are mediated by the decrease in synaptosomal AMPAR level.

To further examine the role of AMPARs in depression, we employed a modified disconnection procedure in mice exposed to subthreshold stress (Fig. 3*P*). Specifically, GABA receptor agonists (27), baclofen and muscimol (B+M), were unilaterally injected into pBLA, and the AMPAR antagonist DNQX (28) was injected into ipsilateral or contralateral vCA1 (the control group received vehicle in both pBLA and vCA1). No significant differences were detected in animals that received ipsilateral B+M and DNQX treatment, while mice that received unilateral intra-pBLA B+M combined with contralateral intra-vCA1 DNQX showed increased immobility time ($F_{4,35} = 3.858$, $P = 0.0106$; Fig. 3 *Q*, *Left*) and decreased latency to immobility in the FST ($F_{4,35} = 2.682$, $P = 0.0474$; Fig. 3 *Q*, *Right*), which recapitulates CUMS-induced depressive-like behavior. These results suggest that inhibition of AMPAR activity in the pBLA-vCA1 innervation could mediate depressive-like behaviors in mice. Overall, our findings indicate that AMPARs play a critical role in CUMS-induced depressive-like behaviors.

CBD Serves as a Major Neuromodulator of pBLA-vCA1 Innervation and Could Alleviate CUMS-Induced Depressive-Like Behavior. Finally, we investigated the neuromodulatory regulation of the pBLA-vCA1 innervation in CUMS-induced depressive-like behavior. It has been reported that endocannabinoids are pivotal endogenous neuromodulators that modulate excitatory/inhibitory (E/I) balance and maintain the neurocircuitry integrity (29). Cannabinoids have shown positive effects for depression treatment, and CBD is considered one of the most promising compounds (30, 31). Therefore, we set to test whether CBD could modulate pBLA-vCA1 innervation under the CUMS procedure (Fig. 4*A*). Although no difference in dendritic complexity ($F_{24,385} = 1.280$, $P = 0.1723$; Fig. 4 *B* and *C*) or total spine number ($F_{4,175} = 5.336$, $P = 0.0004$; Fig. 4*D*) was detected, CBD application could reverse CUMS-induced reduction of mature dendritic spines ($F_{4,175} = 5.657$, $P = 0.0003$; Fig. 4*D*). Moreover, CBD application restored synaptosomal GluA1 level ($F_{4,25} = 5.348$, $P = 0.003$), as well as phosphorylation at S831 in GluA1 ($F_{4,25} = 9.557$, $P < 0.0001$) and T286 in CaMKIIα ($F_{4,25} = 6.553$, $P = 0.0009$; Fig. 4 *E* and *F*). Interestingly, application of AM251, an antagonist of CBD receptor CB_1Rs, resulted in partial block of the CBD effects (Fig. 4 *B–F*), which further demonstrates that CBD administration could lead to changes in pBLA-vCA1 innervation. More importantly, we found that application of CBD significantly activated the vCA1 excitatory neurons innervated by pBLA ($F_{4,20} = 8.807$, $P = 0.0003$; Fig. 4*G*) and reduced the immobility time ($F_{4,35} = 4.361$, $P = 0.0058$) and increased the latency to immobility ($F_{4,35} = 5.808$, $P = 0.0011$) in the FST (Fig. 4*H*). These results show that CBD could modulate the pBLA-vCA1 innervation and alleviate depressive-like behaviors in mice subjected to CUMS.

Discussion

pBLA-vCA1 Innervation in Depression. The brain effectively adapts to stress through modification of the connectivity and strength between synapses and neuronal circuits (32). Notably, the pattern of modification is highly dependent upon stress intensity and duration (33). Acute stress generally produces momentary and bidirectional effects and is normalized quickly (34, 35), while chronic stress produces relatively long-lasting and unidirectional remodeling (36–38). Previous studies have shown that chronic stress could induce region-specific changes and subsequent behavioral and emotional deficits. Brain regions responsible for cognitive and executive control, such as the PFC and hippocampus, show impaired long-term potentiation (LTP) and LTD after longtime stress exposure (39–42). Consistent with functional negative alterations, chronic stress also reduces neurogenesis (41) and induces pyramidal dendrite retraction in hippocampus (43). These negative effects can be reversed by antidepressants (41, 42, 44). Other regions, most notably the BLA, may feature an opposite neuronal pathology (45), although there are reports of negative changes such as pyramidal dendrite atrophy and GluA1 reduction in BLA after chronic stress (9, 46).

These seemingly contradictory pathological changes are thought to be due to the anatomical and functional heterogeneity of BLA along its anterior–posterior axis. There are two types of excitatory pyramidal neurons in the BLA, magnocellular and parvocellular neurons, which are intermingled with interneurons. Anterior BLA consists of magnocellular neurons expressing *R-sPondin 2*, while posterior BLA consists of parvocellular neurons expressing *Protein PhosPhatase 1 regulatory inhibitor subunit 1B*. It has been reported that aBLAs are activated after aversive experience and pBLAs are activated upon rewarding experience (47). There is evidence that optogenetic inhibition of BLA inputs to vHPC reduces anxiety-related behaviors (25), and activation of this circuit decreases sociability in a three-chamber test (48). However, BLA neurons projecting to vHPC do not express obvious preferences for either positive or negative valence. Therefore, understanding the organization and functional alteration of the BLA-vHPC circuit after chronic stress might help to reveal basic principles underlying emotional processing and depression.

Our data demonstrate that CUMS exposure led to decreased activity of excitatory pyramidal neurons in a few brain regions such as vCA1, pBLA, and nucleus accumbens core (Fig. 1 and *SI Appendix*, Fig. S1). We found that pBLA projection to vCA1 played a critical role in CUMS-induced depressive-like behaviors (Fig. 2), which is consistent with previous findings (15, 49). Mice subjected to negative stimuli showed reduced activity of pBLA-vCA1 innervation. Notably, although activated neurons in pBLA mainly project to vCA1, only 46% of activated neurons in vCA1 were innervated by pBLA (Fig. 2 and *SI Appendix*, Fig. S2). These results suggest a multiple-input modulation of neuronal excitability in vCA1 during CUMS exposure, consistent with the fact that vCA1 pyramidal neurons can be divided into diverse

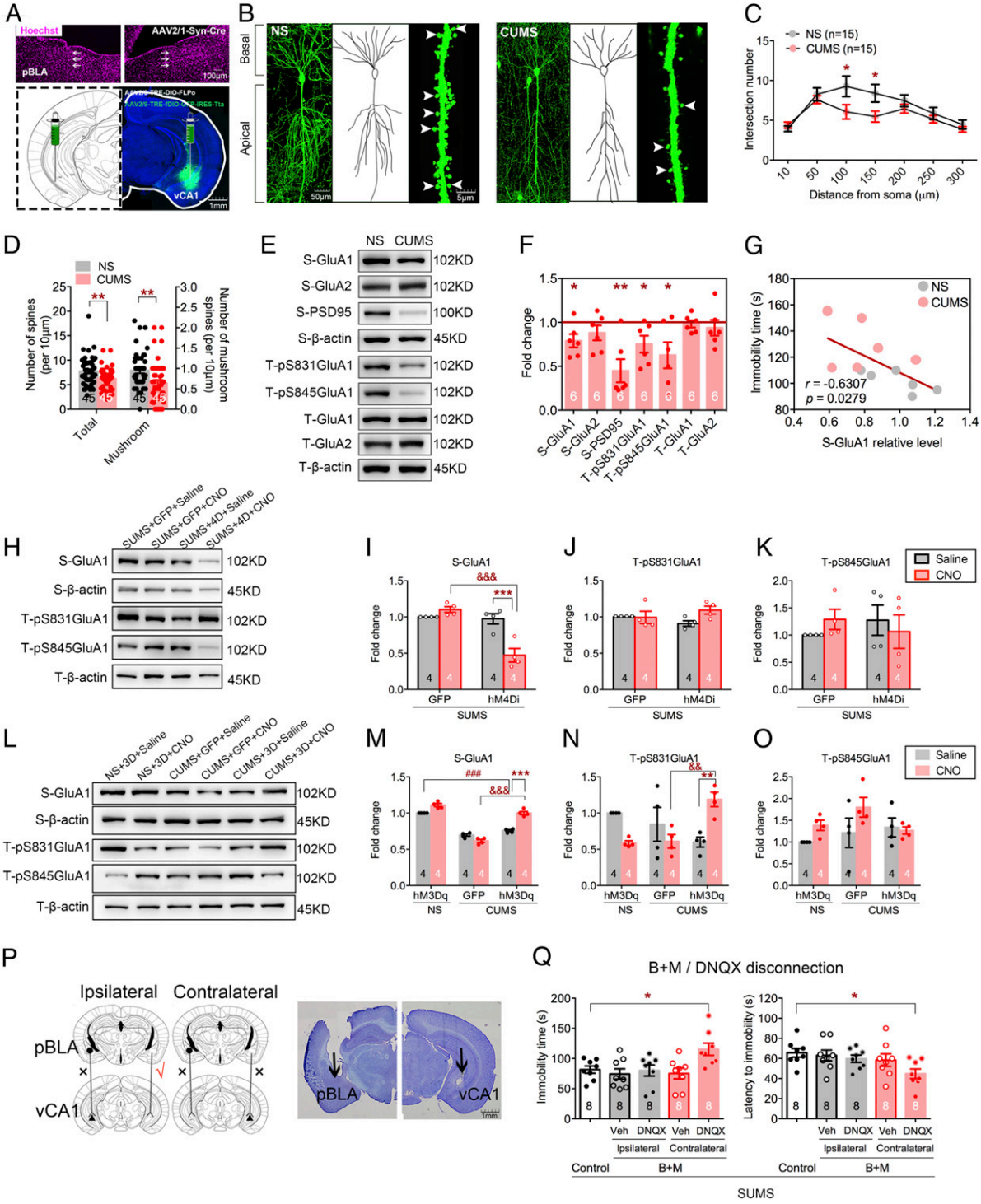

Fig. 3. AMPARs play an important role in CUMS-induced depressive-like behaviors. (*A*) Representative images of Cre-recombinase injection trace (white arrows) in pBLA (*Top*) and Cre/loxP-based Supernova vectors in vCA1 (*Bottom*). (*B*) Representative images of dendrites, traced neuronal processes, and spines in vCA1 in each group. White arrowheads indicate mushroom spines. (*C*) Quantification of dendritic intersection (two-way ANOVA with Sidak's post hoc test, $^{*}P < 0.01$, NS vs. CUMS group; $n = 15$ neurons from $n = 5$ mice per group, Sholl analysis). (*D*) Quantification of total and mushroom spines in vCA1 (unpaired Student's *t* test, $^{**}P < 0.01$; $n = 45$ dendritic segments from $n = 5$ mice per group). (*E*) Representative images of Western blots. (*F*) Quantification of synaptosomal ("S") GluA1, GluA2, and PSD95 and total ("T") pS831GluA1, pS845GluA1, GluA1, and GluA2 in vCA1 (unpaired Student's *t* test, $^{*}P < 0.05$, $^{**}P < 0.01$, CUMS vs. NS group). (*G*) Relationship between synaptosomal GluA1 relative level in vCA1 and immobility time in FST (Pearson's correlation, $r = -0.6307$, $P = 0.0279$; $n = 6$ per group). (*H*) Representative images of Western blots. (*I–K*) Quantification of synaptosomal ("S") GluA1 and total ("T") pS831GluA1 and pS845GluA1 in vCA1 after chemogenetic inhibition (two-way ANOVA with Sidak's post hoc test, $^{***}P < 0.0001$, $^{\&\&\&}P < 0.05$). (*L*) Representative images of Western blots. (*M–O*) Quantification of synaptosomal ("S") GluA1 and total ("T") pS831GluA1 and pS845GluA1 in vCA1 after chemogenetic activation (two-way ANOVA with Sidak's post hoc test, $^{**}P < 0.01$, $^{***}P < 0.0001$, $^{\#\#\#}P < 0.01$, $^{\&\&\&}P < 0.05$). (*P*, *Left*) Disconnection procedure in SUMS mice. (*P*, *Right*) Histological sites of cannula placements in the pBLA and vCA1, respectively. (*Q*) Immobility and latency to immobility in FST after disconnection procedure (one-way ANOVA with Sidak's post hoc test, $^{*}P < 0.05$). Data are presented as the mean ± SEM.

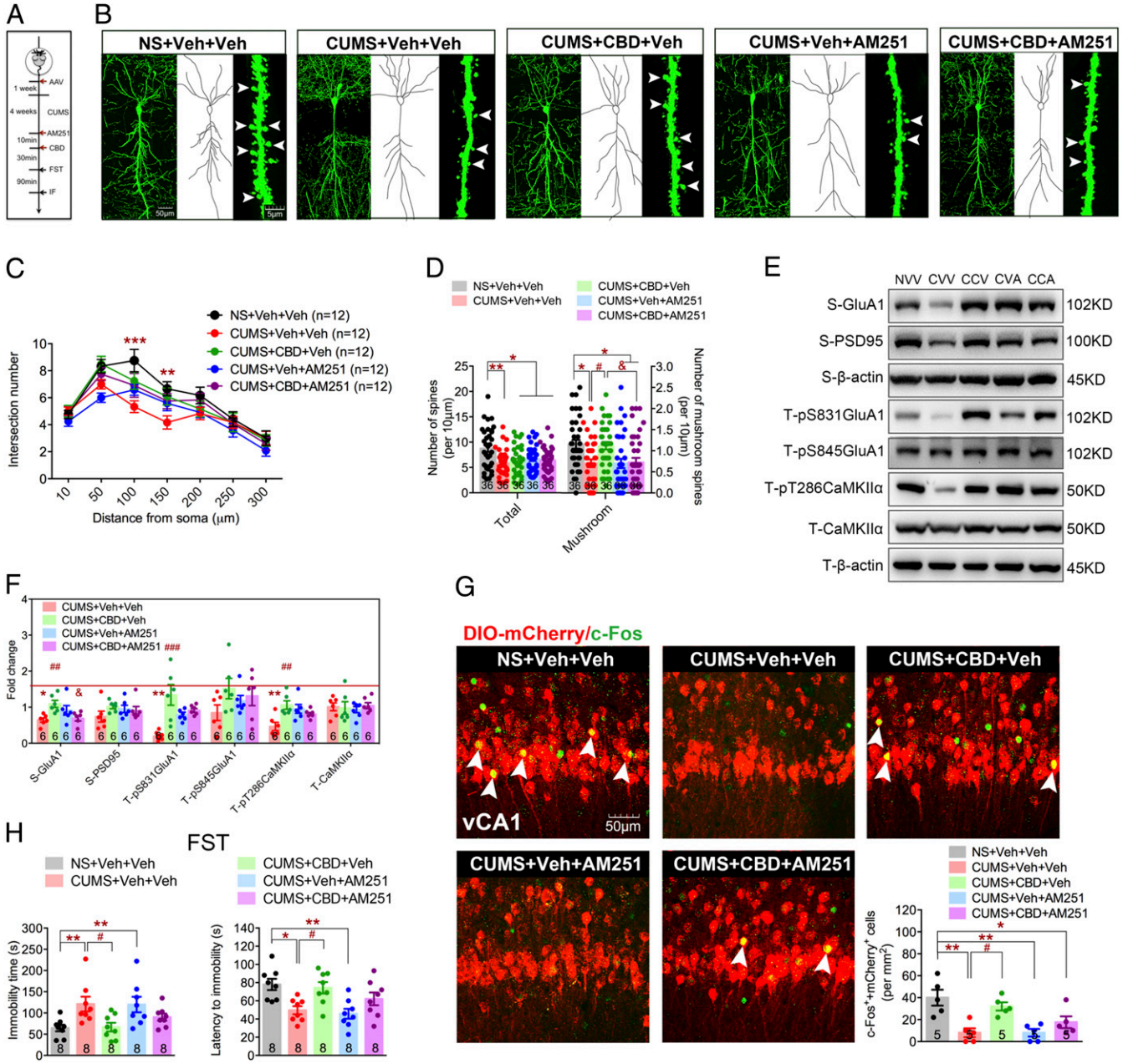

Fig. 4. CBD functions as a neuromodulator of pBLA-vCA1 innervation in CUMS-induced depressive-like behaviors. (*A*) Experimental design. (*B*) Representative images of dendrites, traced neuronal processes, and spines in vCA1 in each group. (*C*) Quantification of dendritic intersection (two-way ANOVA with Sidak's post hoc test, $^{**}P < 0.01$, $^{***}P < 0.001$, NS+Veh+Veh vs. CUMS+Veh+Veh group; $n = 12$ neurons from $n = 4$ mice per group; Sholl analysis). (*D*) Quantification of total and mushroom spines in vCA1 (one-way ANOVA with Tukey's post hoc test, $^{*}P < 0.05$, $^{**}P < 0.01$, $^{\#}P < 0.05$, $^{\&}P < 0.05$; $n = 36$ dendritic segments from $n = 4$ mice per group). (*E*) Representative images of Western blots. NVV, NS+Veh+Veh; CVV, CUMS+Veh+Veh; CCV, CUMS+CBD+Veh; CVA, CUMS+Veh+AM251; CCA, CUMS+CBD+AM251. (*F*) Quantification of synaptosomal ("S") GluA1, GluA2, and PSD95 and total ("T") pS831GluA1, pS845GluA1, pT286CaMKIIα, and CaMKIIα in vCA1 (one-way ANOVA with Tukey's post hoc test, $^{*}P < 0.05$, $^{**}P < 0.01$, CUMS+Veh+Veh vs. NS+Veh+Veh group; $^{\#\#}P < 0.01$, $^{\#\#\#}P < 0.001$, CUMS+CBD+Veh vs. CUMS+Veh+Veh group; $^{\&}P < 0.05$, CUMS+CBD+AM251 vs. CUMS+CBD+Veh group). (*G*) Representative images and quantification of DIO-mCherry (red) and c-Fos (green) double-positive cells in vCA1. White arrowheads indicate colabeled cells (one-way ANOVA with Tukey's post hoc test, $^{*}P < 0.05$, $^{**}P < 0.01$, $^{\#}P < 0.05$). (*H*) Immobility (*Left*) and latency time (*Right*) in FST after CBD treatment (one-way ANOVA with Tukey's post hoc test, $^{*}P < 0.05$, $^{**}P < 0.01$, $^{\#}P < 0.05$). Data are presented as the mean ± SEM.

subpopulations (50). Indeed, recent studies have shown that pBLA mainly innervates superficial-layered Calb1-positive neurons in vCA1 and the pBLA-vCA1^{Calb1+} circuit drives approach behavior to reduce anxiety-like behavior (16). Our data show that chemogenetic activation of pBLA-vCA1 innervation can alleviate the depressive-like behaviors; on the contrary, inhibition of pBLA-vCA1 innervation exacerbated depression phenotypes (Fig. 2 and *SI Appendix*, Fig. S3). These results demonstrate that pBLA-vCA1 innervation plays an important, bidirectional role in an animal model of depression.

Cannabinoid Agents in Depression. Consistent with previous findings, our results showed reduced dendritic complexity and spine density, as well as decreased synaptosomal GluA1 and PSD95 in

vCA1 (Fig. 3). AMPARs play a critical role in synaptic plasticity, and impairments of AMPARs have been indicated in multiple neurological and psychiatric disorders (51). Phosphorylation of S845 increases single-channel open probability, and phosphorylation of S831 increases single-channel conductance (52, 53); these two phosphorylation sites also play a synergistic role in LTP expression. Our data demonstrate CUMS-induced reduction of S831 phosphorylation in vCA1 (Fig. 3), indicating that chronic stress might impair LTP through posttranslational modification of AMPARs. Moreover, blockage of AMPARs in vCA1 combined with contralateral pBLA inactivation could induce a depressive-like phenotype in mice subjected to subthreshold stress, which suggests that AMPAR activity in the pBLA-vCA1 innervation could mediate depressive-like behaviors.

CUMS treatment led to reduced activity of pBLA-vCA1 innervation, which in turn would result in an E/I balance shift in pBLA inputs to vCA1. Previous studies have shown that cannabinoids regulate presynaptic GABA and glutamate release in the brain (54), and the cannabinoid system plays an important role in orchestrating E/I balance and controlling stress responses (55). Recently, cannabinoids, most notably CBD, have shown positive signs for the treatment of emotional disorders such as anxiety and depression (30, 31). We found CBD could promote struggling behavior in the FST 30 min after administration (Fig. 4), indicating a fast-acting antidepressant effect. This observation is consistent with previous reports describing its antidepressant-like effects (56–58) through increased activity of vCA1 neurons receiving inputs from pBLA (Fig. 4). Since fast-acting antidepressants like ketamine and scopolamine work through rapid increase of synaptogenesis (59, 60), we further investigated if CBD would increase the density of dendritic spines and/or synaptic protein levels. Our data showed that acute CBD did not reverse CUMS-induced dendrite spine density decrease or synaptic PSD95 reduction in vCA1. One possible explanation could be that acute CBD rapidly strengthens AMPAR-medicated synaptic connections in pBLA-vCA1 within preexisting spines. It has been shown that plasticity at preexisting stable spines was much more widespread (17). Acute CBD treatment could reverse levels of synaptosomal GluA1 and phosphorylation at S831 in GluA1 and T286 in CaMKIIα in vCA1. CBD treatment was only partially blocked by CB_1R antagonist AM251 (Fig. 4), most likely due to CBD acting on other receptors such as CB_2 and $GABA_A$ receptors (29). Furthermore, previous studies have shown increased dendritic length and branches and PSD95 level after chronic CBD treatment in mice subjected to CUMS (25), which indicates that CBD could have long-term antidepressant effects.

The rapid antidepressant effect of CBD might work through shifting E/I balance in vCA1 by activating pBLA-vCA1 innervation. CBD could silence GABAergic interneurons through presynaptic CB_1Rs and induce a glutamate burst from pBLA inputs, which could reverse CUMS-induced activity decrease of pBLA-vCA1 innervation. Activation of CaMKIIα indicates an increase in intracellular Ca^{2+}; however, the source of calcium entry needs further examination. Activated CaMKIIα can enhance phosphorylation of GluA1 S831 and increase channel activity. Enhanced AMPAR synaptic transmission of pBLA-vCA1 innervation could alleviate depressive-like behaviors induced by chronic stress (29). The underlying mechanisms of sustained and long-term effects of CBD need to be investigated in future studies.

We have demonstrated that pBLA-vCA1 innervation plays a critical role in a CUMS-induced animal model of depression and that CBD treatment can reverse depression-related changes in activity and synaptosomal AMPAR expression at pBLA-vCA1 synapses and alleviate depressive-like behaviors in mice. Thus, manipulating the activity of pBLA-vCA1 innervation using compounds like CBD could be a promising approach for potential depression treatment.

Materials and Methods

Animals. Young male adult C57BL/6 (6 to 8 wk of age) and CaMKII-Cre mice were used for our studies. CaMKII-Cre mice were a gift from Chen Zhang's lab at Capital Medical University (Beijing, China). Mice were housed four to five per cage under a 12-h light/dark cycle (light on from 7 AM to 7 PM) with free access to food and water ad libitum, while the animals under the CUMS procedure were housed individually. All animal studies and experimental procedures were approved by the animal care and use committee of the animal facility at Peking University Health Science Center.

Virus and Drugs. All the viruses used in our study were purchased from OBiO Technology: AAV2/9-CaMKIIα-hM3D(Gq)-mCherry (4.39×10^{12} viral genomes per mL [V.G./mL], 0.3 μL per site), AAV2/9-CaMKIIα-mCherry (4.68×10^{12} V.G./mL, 0.3 μL per site), AAV2/1-Ef1a-DIO-mCherry-WPRE (3.92×10^{13} V.G./mL, 0.2 μL per site), AAV2/9-hSyn-DIO-hM3D(Gq)-GFP (1.46×10^{13} V.G./mL, 0.2 μL per site), AAV2/9-hSyn-DIO-hM4D(Gi)-GFP (1.41×10^{13} V.G./mL, 0.2 μL per site), AAV2/9-hSyn-DIO-GFP (2.11×10^{13} V.G./mL, 0.2 μL per site), AAV2/Retro-CaMKIIα-mCherry-Cre (3.2×10^{12} V.G./mL, 0.3 μL per site), AAV2/1-hSyn-Cre (1.34×10^{13} V.G./mL, 0.2 μL per site), AAV2/9-TRE-DIO-FLPo (9.72×10^{12} V.G./mL), and AAV2/9-TRE-fDIO-GFP-IRES-Tta (6.21×10^{12} V.G./mL) mixed in the ratio of 1:100 (total 0.3 μL per site). Drugs used in our experiments were as follows: CNO (5.0 mg/kg in 0.9% saline; ab141704; Abcam), Fluoro-Gold (i.e., FG; 4% in 0.9% saline, 0.2 μL per site; Fluoro-001; Fluorochrome), baclofen (G014; Sigma) and muscimol (G019; Sigma) mixed in the ratio of 1:1 (total 250 ng/μL in 0.9% saline, 0.2 μL per side), DNQX (5 μg/μL in 0.9% saline; 0.3 μL per side; no. 0189; Tocris), CBD (30 mg/kg in 2% Tween-80 in 0.9% saline; E3691; Lableader), and AM251 (0.3 mg/kg in 2% Tween-80 in 0.9% saline; no. 1117; Tocris).

CUMS. The CUMS procedure was adopted from a previous study (61). In brief, mice were exposed to randomized stressors twice a day (at 9 AM to 11 AM and 2 PM to 4 PM, respectively) over 4 wk, including 24-h water/food deprivation, 24-h soiled/empty cage, 24-h cage tilt (30°), reversed light/dark cycle, overnight illumination, 2-h paired housing, 1.5-h confinement, 15-min restraint stress, 10-min cold stress at 4 °C, and 5-min cold swimming. No same stressor was applied in succession. For the SUMS procedure, mice were subjected to the CUMS procedure for 1 wk instead of 4 wk. NS mice were housed under normal conditions (four to five per cage) and only switched to individual housing during the depressive-like behavior testing phase.

Behavioral Tests. All behavioral tests were performed during the light phase (11:00 AM to 5:00 PM), and mice were housed individually. For SPT, mice were water-deprived for 16 h, then given access to two preweighed bottles with stoppers fitted with ballpoint sipper tubes for 90 min, one containing drinking water and the other containing 1.5% sucrose solution. The positions (left or right) of water and sucrose were switched every 30 min to ensure that the mice did not develop a side preference. Bottles were weighed again after 30 min, and the weight difference during the last 60 min was used for calculation. Sucrose preference was measured as the percentage of sucrose intake over total water and sucrose intake. For NSFT, after a 24-h food deprivation and adaption to the environment for 30 min, mice were individually placed into an open field ($40 \times 40 \times 50$ cm) with food pellets placed in the center. The time until the first feeding episode was video-recorded for 5 min. Mice were then returned to their home cage, and the food consumption was measured for 60 min. For FST, mice were individually placed in a vertical transparent cylinder (20 cm height × 14 cm diameter) with 13-cm-deep water (23 to 24 °C) for 6 min after adapting to the environment for 30 min. The duration and latency of immobility were video-recorded during the last 5 min.

Surgery. Mice were anesthetized with 1.2% avertin (0.2 mL/10 g, i.p.) and head-fixed in a stereotaxic apparatus (RWD Life Science). For cannula implantation, stainless steel guide cannulas (0.41 mm in outer diameter) were bilaterally implanted above the pBLA [anteroposterior (AP), −2.18 mm; mediolateral (ML), ±3.10 mm; dorsoventral (DV), −4.50 mm; AP, −2.18 mm, ML, ±3.10 mm; DV, −4.40 mm; Fig. 3 *P* and *Q*] and vCA1 (AP, −3.16 mm; ML, ±2.95 mm; DV, −4.15 mm; AP, −3.28 mm; ML, ±3.10 mm: DV; −4.40 mm; Fig. 3 *P* and *Q*) through a small hole drilled on the skull. Guide cannulas were fixed to the skull with dental cement. Stainless steel obturators were inserted into the guide cannulas to keep it unobstructed and prevent infection. During intracranial injection, the obturators were removed, and injection cannulas (0.21 mm in outer diameter) were inserted. The injection cannulas were connected to 1-μL Hamilton syringes via polyethylene (PE) tubing (0.85 mm in outer diameter), which was back-filled with saline, with a

small air bubble separating the saline from the drug or vehicle. The cannulas were left in place for an additional 5 min after injection to allow drug diffusion. The obturators were then reinserted. For direct microinjection through a syringe, a small hole was drilled on the skull, and the viruses or drugs were delivered with a syringe pump. The coordinates were measured from bregma according to the Mouse Atlas (62). We injected at a rate of 0.05 μL/min, and the syringe was left in place for an additional 5 min before it was slowly withdrawn. Mice were given 1 wk for recovery.

Immunofluorescence Staining. Mice were anesthetized with 1.2% avertin (0.2 mL/10 g) i.p. injection 90 min after FST and perfused transcardially with 0.9% saline followed by 4% paraformaldehyde [in 0.1 M phosphate-buffered saline (PBS) solution, pH 7.4]. The brains were removed and postfixed in 4% paraformaldehyde for 24 h at 4 °C before they were dehydrated subsequently in 20% and 30% sucrose (in 0.1 M PBS, pH 7.4). Coronal sections (30 μm thick) were prepared using a cryostat microtome (model 1950; Leica). The sections were permeabilized with PBST (0.1 M PBS with 0.3% Triton X-100) for 30 min and then blocked with PBST containing 5% normal goat serum for 1 h at room temperature. Then, the sections were incubated with the primary antibody in PBST with 1% normal goat serum overnight at 4 °C. The following primary antibodies were used in our experiments: rabbit anti–c-Fos (1:500; sc-52, Santa Cruz Biotechnology), mouse anti-NeuN (1:800; MAB377, Millipore), mouse anti-CaMKIIα (1:500; sc-13141, Santa Cruz Biotechnology), mouse anti-GAD67 (1: 500; MAB5406, Millipore), and mouse anti-PV (1:500; PV235, Swant). The sections were then washed three times in PBST and incubated with indicated secondary antibodies for 1.5 h at room temperature. The following secondary antibodies were used in our experiments: Alexa Fluor 488 goat anti-rabbit IgG (for c-Fos, 1:500; ab150077, Abcam), Alexa Fluor 594 goat anti-mouse IgG (for NeuN 1:500; ab150116, Abcam), Alexa Fluor 405 goat anti-mouse IgG (for NeuN 1:500; ab175660, Abcam), and Hoechst 33258 (1:500; H3569, Invitrogen). Finally, after three more washes with PBST, the sections were mounted on antifade medium (C1210, Applygen Technologies) and imaged by confocal microscope (Olympus FV1000). All images were acquired at 1,024 × 1,024 resolution using 3× Kalman frame averaging. High-resolution *z*-stacks were acquired using a 60× oil-immersion lens (numerical aperture, 1.49; with 3× optical zoom for dendritic branch segments) at a step size of 1 μm. For quantification of double- or triple-positive cells, three sections were selected in aBLA (from 1.22 mm to 1.82 mm posterior to bregma), pBLA (from 2.18 mm to 2.80 mm posterior to bregma), or vCA1 (from 2.92 mm to 3.52 mm posterior to bregma) from an individual animal and counted manually in a double-blind manner.

Sholl Analysis and Dendritic Spine Counting. Sholl analysis was carried out as described previously (63). Coronal sections (50 μm thick) were processed for imaging. Confocal *z*-stacks of GFP^+ cells were taken from each vCA1 (from 2.92 mm to 3.52 mm posterior to bregma) section per mouse. Images were imported into Adobe Illustrator CS5, and dendritic trees were reconstructed using the tracing tool. Dendritic complexity was analyzed from 8-bit images using ImageJ. The center of the soma was defined as the center of all concentric circles. The parameters used were starting radius (10 μm from the center), ending radius (300 μm), and interval between consecutive radii (10 μm). Three pyramidal neurons were randomly selected from individual animal for Sholl analysis. Three secondary or tertiary dendritic branch segments longer than 40 μm were randomly selected from individual cells for spine counting. Mushroom spines are defined as a head diameter larger than 0.5 μm and a head-to-neck diameter ratio greater than 1:1.

Western Blotting. Mice were euthanized immediately after behavioral tests, and the brains were quickly removed and frozen until further analysis. Coronal sections were prepared in a cryostat microtome after fixation, and bilateral vCA1s were dissected carefully with a no. 8 blunt puncture needle from sections between 2.92 mm and 3.80 mm posterior to bregma. Purified synaptosomes were extracted according to a previous study (64). vCA1 was dissected and homogenized in a precooling buffer containing 320 mM sucrose, 20 mM Hepes, 1 mM EDTA, and 1× protease inhibitor mix. The homogenate was centrifuged for 10 min at 2,800 rpm at 4 °C. Twenty microliters of the supernatant (S1) was preserved for total protein analysis, and the remaining was further centrifuged for 10 min at 12,000 rpm at 4 °C, producing the pellet (crude synaptosomal fraction, P2). P2 was resuspended in RIPA buffer (C1035, Applygen Technologies) with 1× protease inhibitor mix. Protein concentration was determined by BCA protein assay (Pierce). Equal amounts of proteins (10 μg) for each sample were loaded for Western blot. The blots were blocked with 5% nonfat milk in TBST (TBS with 0.1% Tween-20) for 1 h at room temperature and then incubated with primary antibody overnight at 4 °C. The following primary antibodies were used in our experiments: rabbit anti-GluA1 (1:2,000; ab109450, Abcam), rabbit anti-GluA2 (1:2,000; ab206293, Abcam), rabbit anti-pS845GluA1 (1:1,000; 8084S, Cell Signaling Technology), rabbit anti-pS831GluA1 (1:1,000; no. 04823, Millipore), rabbit anti-PSD95 (1:1,000; ab18258, Abcam), rabbit anti-pT286CaMKII (1:1,000; 12716S, Cell Signaling Technology), mouse anti-CaMKII (1:1,000; sc-13141, Santa Cruz Biotechnology), and rabbit anti–β-actin (1:1,000; 4970S, Cell Signaling Technology). The blots were washed three times in TBST and incubated with horseradish peroxidase-conjugated goat anti-rabbit (1:2,000; ZB-2301, Zhongshan Biotechnology) or goat anti-mouse (1:2,000; ZB-2305, Zhongshan Biotechnology) secondary antibodies for 1 h at room temperature. After the final three washes with TBST, the blots were detected using a chemiluminescence detection kit (WBKLS0500, Millipore) and analyzed quantitatively by densitometry with Quantity One 1-D analysis software. β-Actin was used as an internal control, and relative expression was normalized to the mean value of control group for each protein.

Statistical Analysis. Statistical analysis was performed using GraphPad Prism. Normally distributed data were tested by one-way or two-way ANOVA followed by post hoc multiple comparison test or unpaired Student's *t* test for two-group comparisons as indicated in figure legends.

Data Availability. All study data are included in the article and/or supporting information.

ACKNOWLEDGMENTS. We thank Drs. Richard Huganir, Brad Pfeiffer, and Yan Zeng for helpful discussion and critical reading of the manuscript; we thank Drs. Jianwei Jiao, Chen Zhang, and Wei Lu for experimental support. This work was supported by National Key R&D Program of China (Grant 2017YFE0103400), the National Natural Science Foundation of China (Grants 31771125, 31790911, and 81521063), and the China Postdoctoral Science Foundation (2020M670059).

1. L. Pezawas *et al*., 5-HTTLPR polymorphism impacts human cingulate-amygdala interactions: A genetic susceptibility mechanism for depression. *Nat. Neurosci.* **8**, 828–834 (2005).
2. K. J. Ressler, H. S. Mayberg, Targeting abnormal neural circuits in mood and anxiety disorders: From the laboratory to the clinic. *Nat. Neurosci.* **10**, 1116–1124 (2007).
3. H. Hu, Reward and aversion. *Annu. Rev. Neurosci.* **39**, 297–324 (2016).
4. S. J. Russo, E. J. Nestler, The brain reward circuitry in mood disorders. *Nat. Rev. Neurosci.* **14**, 609–625 (2013).
5. C. D. Proulx, O. Hikosaka, R. Malinow, Reward processing by the lateral habenula in normal and depressive behaviors. *Nat. Neurosci.* **17**, 1146–1152 (2014).
6. D. W. Roddy *et al*., The Hippocampus in depression: More than the sum of its parts? Advanced hippocampal substructure segmentation in depression. *Biol. Psychiatry* **85**, 487–497 (2019).
7. W. N. Marsden, Synaptic plasticity in depression: Molecular, cellular and functional correlates. *Prog. Neuropsychopharmacol. Biol. Psychiatry* **43**, 168–184 (2013).
8. A. J. Kallarackal *et al*., Chronic stress induces a selective decrease in AMPA receptor-mediated synaptic excitation at hippocampal temporoammonic-CA1 synapses. *J. Neurosci.* **33**, 15669–15674 (2013).
9. J. Kim, M. Pignatelli, S. Xu, S. Itohara, S. Tonegawa, Antagonistic negative and positive neurons of the basolateral amygdala. *Nat. Neurosci.* **19**, 1636–1646 (2016).
10. M. G. McKernan, P. Shinnick-Gallagher, Fear conditioning induces a lasting potentiation of synaptic currents in vitro. *Nature* **390**, 607–611 (1997).
11. M. T. Rogan, U. V. Stäubli, J. E. LeDoux, Fear conditioning induces associative long-term potentiation in the amygdala. *Nature* **390**, 604–607 (1997).
12. S. Rumpel, J. LeDoux, A. Zador, R. Malinow, Postsynaptic receptor trafficking underlying a form of associative learning. *Science* **308**, 83–88 (2005).
13. K. M. Tye, G. D. Stuber, B. de Ridder, A. Bonci, P. H. Janak, Rapid strengthening of thalamo-amygdala synapses mediates cue-reward learning. *Nature* **453**, 1253–1257 (2008).
14. K. M. Tye *et al*., Methylphenidate facilitates learning-induced amygdala plasticity. *Nat. Neurosci.* **13**, 475–481 (2010).
15. Y. Yang *et al*., Opposite monosynaptic scaling of BLP-vCA1 inputs governs hopefulness- and helplessness-modulated spatial learning and memory. *Nat. Commun.* **7**, 11935 (2016).
16. G. Pi *et al*., Posterior basolateral amygdala to ventral hippocampal CA1 drives approach behaviour to exert an anxiolytic effect. *Nat. Commun.* **11**, 183 (2020).
17. Y. Zhang, R. H. Cudmore, D. T. Lin, D. J. Linden, R. L. Huganir, Visualization of NMDA receptor-dependent AMPA receptor synaptic plasticity in vivo. *Nat. Neurosci.* **18**, 402–407 (2015).
18. A. Barbon *et al*., Chronic antidepressant treatments induce a time-dependent up-regulation of AMPA receptor subunit protein levels. *Neurochem. Int.* **59**, 896–905 (2011).
19. W. Jiang *et al*., Cannabinoids promote embryonic and adult hippocampus neurogenesis and produce anxiolytic- and antidepressant-like effects. *J. Clin. Invest.* **115**, 3104–3116 (2005).

20. F. R. Bambico, N. Katz, G. Debonnel, G. Gobbi, Cannabinoids elicit antidepressant-like behavior and activate serotonergic neurons through the medial prefrontal cortex. *J. Neurosci.* **27**, 11700–11711 (2007).
21. A. C. Campos *et al*., The anxiolytic effect of cannabidiol on chronically stressed mice depends on hippocampal neurogenesis: Involvement of the endocannabinoid system. *Int. J. Neuropsychopharmacol.* **16**, 1407–1419 (2013).
22. M. V. Fogaça, A. C. Campos, L. D. Coelho, R. S. Duman, F. S. Guimarães, The anxiolytic effects of cannabidiol in chronically stressed mice are mediated by the endocannabinoid system: Role of neurogenesis and dendritic remodeling. *Neuropharmacology* **135**, 22–33 (2018).
23. P. Willner, The chronic mild stress (CMS) model of depression: History, evaluation and usage. *Neurobiol. Stress* **6**, 78–93 (2016).
24. D. Knowland, B. K. Lim, Circuit-based frameworks of depressive behaviors: The role of reward circuitry and beyond. *Pharmacol. Biochem. Behav.* **174**, 42–52 (2018).
25. A. C. Felix-Ortiz *et al*., BLA to vHPC inputs modulate anxiety-related behaviors. *Neuron* **79**, 658–664 (2013).
26. R. Lin *et al*., Cell-type-specific and projection-specific brain-wide reconstruction of single neurons. *Nat. Methods* **15**, 1033 (2018).
27. J. R. St Onge, S. B. Floresco, Prefrontal cortical contribution to risk-based decision making. *Cereb. Cortex* **20**, 1816–1828 (2010).
28. C. J. Shen *et al*., Cannabinoid CB1 receptors in the amygdalar cholecystokinin glutamatergic afferents to nucleus accumbens modulate depressive-like behavior (vol 25, pg 337, 2019). *Nat. Med.* **25**, 350 (2019).
29. M. V. Fogaça, R. S. Duman, Cortical GABAergic dysfunction in stress and depression: New insights for therapeutic interventions. *Front. Cell. Neurosci.* **13**, 87 (2019).
30. E. Poleszak *et al*., Cannabinoids in depressive disorders. *Life Sci.* **213**, 18–24 (2018).
31. M. Stampanoni Bassi *et al*., Exploiting the multifaceted effects of cannabinoids on mood to boost their therapeutic use against anxiety and depression. *Front. Mol. Neurosci.* **11**, 424 (2018).
32. M. Joëls, Z. Pu, O. Wiegert, M. S. Oitzl, H. J. Krugers, Learning under stress: How does it work? *Trends Cogn. Sci.* **10**, 152–158 (2006).
33. M. J. A. G. Henckens, G. A. van Wingen, M. Joëls, G. Fernández, Time-dependent effects of corticosteroids on human amygdala processing. *J. Neurosci.* **30**, 12725–12732 (2010).
34. E. Y. Yuen *et al*., Acute stress enhances glutamatergic transmission in prefrontal cortex and facilitates working memory. *Proc. Natl. Acad. Sci. U.S.A.* **106**, 14075–14079 (2009).
35. Z. P. Liu *et al*., Chronic stress impairs GABAergic control of amygdala through suppressing the tonic GABAA receptor currents. *Mol. Brain* **7**, 32 (2014).
36. S. Chattarji, A. Tomar, A. Suvrathan, S. Ghosh, M. M. Rahman, Neighborhood matters: Divergent patterns of stress-induced plasticity across the brain. *Nat. Neurosci.* **18**, 1364–1375 (2015).
37. E. Dias-Ferreira *et al*., Chronic stress causes frontostriatal reorganization and affects decision-making. *Science* **325**, 621–625 (2009).
38. A. F. T. Arnsten, Stress signalling pathways that impair prefrontal cortex structure and function. *Nat. Rev. Neurosci.* **10**, 410–422 (2009).
39. D. N. Alfarez, M. Joëls, H. J. Krugers, Chronic unpredictable stress impairs long-term potentiation in rat hippocampal CA1 area and dentate gyrus in vitro. *Eur. J. Neurosci.* **17**, 1928–1934 (2003).
40. R. Holderbach, K. Clark, J. L. Moreau, J. Bischofberger, C. Normann, Enhanced long-term synaptic depression in an animal model of depression. *Biol. Psychiatry* **62**, 92–100 (2007).
41. P. Niehusmann *et al*., Coincidence detection and stress modulation of spike time-dependent long-term depression in the hippocampus. *J. Neurosci.* **30**, 6225–6235 (2010).
42. K. M. Christian, A. D. Miracle, C. L. Wellman, K. Nakazawa, Chronic stress-induced hippocampal dendritic retraction requires CA3 NMDA receptors. *Neuroscience* **174**, 26–36 (2011).
43. H. J. Krugers, P. M. Goltstein, S. van der Linden, M. Joëls, Blockade of glucocorticoid receptors rapidly restores hippocampal CA1 synaptic plasticity after exposure to chronic stress. *Eur. J. Neurosci.* **23**, 3051–3055 (2006).
44. L. Eiland, J. Ramroop, M. N. Hill, J. Manley, B. S. McEwen, Chronic juvenile stress produces corticolimbic dendritic architectural remodeling and modulates emotional behavior in male and female rats. *Psychoneuroendocrinology* **37**, 39–47 (2012).
45. J. Gilabert-Juan, E. Castillo-Gomez, M. Pérez-Rando, M. D. Moltó, J. Nacher, Chronic stress induces changes in the structure of interneurons and in the expression of molecules related to neuronal structural plasticity and inhibitory neurotransmission in the amygdala of adult mice. *Exp. Neurol.* **232**, 33–40 (2011).
46. A. Chandran *et al*., Reduced phosphorylation of the mTOR signaling pathway components in the amygdala of rats exposed to chronic stress. *Prog. Neuropsychopharmacol. Biol. Psychiatry* **40**, 240–245 (2013).
47. A. Beyeler *et al*., Divergent routing of positive and negative information from the amygdala during memory retrieval. *Neuron* **90**, 348–361 (2016).
48. H. W. Dong, L. W. Swanson, L. Chen, M. S. Fanselow, A. W. Toga, Genomic-anatomic evidence for distinct functional domains in hippocampal field CA1. *Proc. Natl. Acad. Sci. U.S.A.* **106**, 11794–11799 (2009).
49. H. Luo *et al*., Virus-mediated overexpression of ETS-1 in the ventral hippocampus counteracts depression-like behaviors in rats. *Neurosci. Bull.* **35**, 1035–1044 (2019).
50. T. Patriarchi, O. R. Buonarati, J. W. Hell, Postsynaptic localization and regulation of AMPA receptors and Cav1.2 by β2 adrenergic receptor/PKA and Ca^{2+}/CaMKII signaling. *EMBO J.* **37**, e99771 (2018).
51. R. L. Huganir, R. A. Nicoll, AMPARs and synaptic plasticity: The last 25 years. *Neuron* **80**, 704–717 (2013).
52. G. H. Diering, R. L. Huganir, The AMPA receptor code of synaptic plasticity. *Neuron* **100**, 314–329 (2018).
53. M. V. Fogaça *et al*., Fine-tuning of defensive behaviors in the dorsal periaqueductal gray by atypical neurotransmitters. *Braz. J. Med. Biol. Res.* **45**, 357–365 (2012).
54. M. N. Hill *et al*., Recruitment of prefrontal cortical endocannabinoid signaling by glucocorticoids contributes to termination of the stress response. *J. Neurosci.* **31**, 10506–10515 (2011).
55. T. V. Zanelati, C. Biojone, F. A. Moreira, F. S. Guimarães, S. R. L. Joca, Antidepressant-like effects of cannabidiol in mice: Possible involvement of 5-HT1A receptors. *Br. J. Pharmacol.* **159**, 122–128 (2010).
56. R. Linge *et al*., Cannabidiol induces rapid-acting antidepressant-like effects and enhances cortical 5-HT/glutamate neurotransmission: Role of 5-HT1A receptors. *Neuropharmacology* **103**, 16–26 (2016).
57. A. P. Schiavon, J. M. Bonato, H. Milani, F. S. Guimarães, R. M. Weffort de Oliveira, Influence of single and repeated cannabidiol administration on emotional behavior and markers of cell proliferation and neurogenesis in non-stressed mice. *Prog. Neuropsychopharmacol. Biol. Psychiatry* **64**, 27–34 (2016).
58. A. E. Autry *et al*., NMDA receptor blockade at rest triggers rapid behavioural antidepressant responses. *Nature* **475**, 91–95 (2011).
59. R. J. Liu *et al*., Brain-derived neurotrophic factor Val66Met allele impairs basal and ketamine-stimulated synaptogenesis in prefrontal cortex. *Biol. Psychiatry* **71**, 996–1005 (2012).
60. H. W. Kessels, R. Malinow, Synaptic AMPA receptor plasticity and behavior. *Neuron* **61**, 340–350 (2009).
61. F. Higuchi *et al*., Hippocampal MicroRNA-124 enhances chronic stress resilience in mice. *J. Neurosci.* **36**, 7253–7267 (2016).
62. G. Paxinos, K. B. J. Franklin, *The Mouse Brain in Stereotaxic Coordinates* (Gulf Professional Publishing, 2004).
63. H. L. Zhang *et al*., Dentate gyrus mu-opioid receptor-mediated neurogenic processes are associated with alterations in morphine self-administration. *Sci. Rep.*, **9** (2019).
64. N. Li *et al*., mTOR-dependent synapse formation underlies the rapid antidepressant effects of NMDA antagonists. *Science* **329**, 959–964 (2010).